Letters in Applied NanoBioScience
Open-Access Journal (ISSN: 2284-6808)

Article
Volume 13, Issue 1, 2024, 49
https://doi.org/10.33263/LIANBS131.049

Enhancing the inhibition action of acetamide with iodide ions for mild steel corrosion in 0.5 M H_2SO_4 environment

Terngu Timothy Uzah [1,*], Idongesit Justina Mbonu [1]

[1] Department of Chemistry, College of Science, Federal University of Petroleum Resources, Effurum, Nigeria. uzah2t@gmail.com (T.T.U); mbonu.idongesit@fupre.edu.ng (I.J.M);
* Correspondence: uzah2t@gmail.com;

Scopus Author ID -

Received: 10.02.2023; Accepted: 28.05.2023; Published: 30.03.2024

Abstract: The inhibitory activity of acetamide and iodide ions was assessed at various concentrations towards mild steel corrosion in 0.5 M H_2SO_4 solution, using electrochemical impedance spectroscopy (EIS) and weight loss studies. SEM (scanning electron microscope) and FTIR analysis were used to investigate corresponding mild steel surfaces. The experimental findings are generally in agreement and show that KI and acetamide have a beneficial synergistic effect that could successfully prevent mild steel from corroding. The inhibitory mechanism of acetamide on the steel surface was further clarified using quantum chemical calculations and Monte Carlo simulation.

Keywords: Mild steel; Acetamide; EIS; Synergistic; Iodide ion; H_2SO_4

© 2024 by the authors. This article is an open-access article distributed under the terms and conditions of the Creative Commons Attribution (CC BY) license (https://creativecommons.org/licenses/by/4.0/).

1. Introduction

One of the biggest issues with petroleum operations is the corrosion of materials, which results in significant financial losses. The environment in which metallic industrial structures are frequently exposed makes corrosive processes easier [1-3]. The petroleum industry uses acid solutions to pickle, acid-clean, and descale steel components [4,5]. To prevent corrosion of the base metal, acidizing inhibitors are added. A potential remedy for corrosion prevention is the use of organic inhibitors [6]. These organic inhibitors are typically electrostatically bound to the metal surface or formed into a coordinate covalent bond (chemical adsorption) before being deposited there (physical adsorption). These substances produced an insoluble complex or were adsorbed onto the metal surface, blocking the active corrosion sites [7]. Previous research has demonstrated that adsorption primarily depends on the p- or d-electrons and the heteroatom of the molecule, which causes more inhibitor molecules to bind to the surface of mild steel. Most organic compounds with high electron density heteroatoms, such as phosphorus, sulfur, nitrogen, and oxygen, used as adsorption sites, are efficient metal corrosion inhibitors [8–11]. The effectiveness of amide compounds as organic corrosion inhibitors has recently been the subject of numerous studies [12–14]. However, interest in using metal corrosion inhibitors has expanded beyond simple prevention to include an inhibitor's potency level.

Corrosion inhibitors can be divided into three categories based on their percentage inhibition efficiency (% IE): poor (% IE 40), moderate (% IE 40–69), and excellent (% IE > 70). [15]. Finding substances that can exert synergistic effects when combined with inhibitors to reduce the quantity of an expensive inhibitor or increase the efficiency of a moderately

performed inhibitor has been one of the steps corrosion scientists have taken in recent years to address the challenges of poor or moderate inhibiting ability of an inhibitor and that of exorbitant price [16–18]. In this work, the impact of KI addition on acetamide's ability to suppress corrosion in mild steel at various concentrations in 0.5 M H_2SO_4 solution at 298-328 K was examined. SEM, quantum chemical calculations, mass loss, electrochemical impedance methods, and Monte Carlo simulation analyses were investigated.

2. Materials and Methods

2.1. Medium.

In a 0.5 M H_2SO_4 solution, the solubility of acetamide and KI (Tianjin Kermel chemical reagent company, China) was assessed. In order to create the 0.5 M corrosive environment, analytical-grade sulfuric acid was diluted with double-distilled water. The measurements were carried out at varied concentrations of $2 \times 10^{-4}, 4 \times 10^{-4}, 6 \times 10^{-4}, 8 \times 10^{-4}$ *and* 1×10^{-3} M) and 5 mM KI, with an immersion time of 6 h, both with and without the addition of acetamide. Additionally, the impact of temperature (298, 308, 318, and 328 K) was investigated for 6 h while immersed in various inhibitor doses.

2.2. Mild Steel.

The mild steel sample elemental analysis that was utilized for the measurements has a composition of manganese (0.56), phosphorus (0.04), carbon (0.27), silicon (0.25), and sulfur (0.04) with balancing Fe.

2.3. Weight-Loss Measurements.

The methods outlined in this article were used to conduct the conventional weight-loss measurements [19]. Cleansed, polished, and weighed mild steel specimens (4.1 x 2.1 x 0.08 cm) were submerged in a 0.5 M H_2SO_4 environment in the absence and presence of various concentrations of the tested inhibitor for 6 hours at temperatures between 298 and 328 K. Each measurement was made three times to guarantee that the tests could be repeated, and only the average results were released. Equations (1) - (3) were used to compute the corrosion rate and inhibition effectiveness.

$$Corrosion\ Rate(C_R) = \frac{W_o - W_1}{At}\ (mg\ cm^{-2}\ min^{-1})\ (1)$$

where, A is the total exposed area in cm^2, W_o is the initial weight before immersion, W_1 is the final weight after immersion, t is the exposed time in minutes.

$$Surface\ coverage\ (S_c) = (1 - \frac{[W]_{inh}}{[W]_{uninh}})(2)$$

$$Percentage\ inhibition\ efficiency\ (\%\ I.E) = S_c \times 100(3)$$

where $[W]_{uninh}$= weight loss in the absence of inhibitors, $[W]_{inh}$= weight loss in the presence of inhibitors

2.4. Electrochemical Data.

Coupons made of mild steel were cleaned in accordance with ASTM standard G1-03 [20] and used as working electrodes throughout the study. The active surface area of the coupon was 4.5 cm2. The tests were conducted with inhibitor doses ranging from 2×10^{-4} to

$1 \times 10^{-3}\ M$ in a 0.5 M H_2SO_4 environment that was aerated but not stirred. Each measurement was made three times to guarantee that the tests could be repeated, and only the average results were released.

The measurements were performed using a BioLogic VMP potentiostat electrochemical analyzer model SP- 300 with EC- Lab software. The inhibitory effects of the tested inhibitor were evaluated using a conventional three-electrode jacketed glass cell with three electrodes: the working electrode (a mild steel coupon), the counter electrode (graphite), and the reference electrode (Ag/AgCl (3 M KCl)). In the current investigation, all potentials were evaluated in relation to Ag/AgCl (3 M KCl). Electrochemical experiments were initiated about 30 minutes after the working electrode was immersed in the solution to maintain the steady-state potential. Three different runs of the same experiment were done to ensure good repeatability. [7,21]

2.5. Scanning electron microscopy (SEM).

The corrosive effects of the acidic solution (0.5 M H_2SO_4) on the mild-steel surface were seen using scanning electron microscopy following treatments lasting 6 hours without and with the addition of $1 \times 10^{-3}\ M$ of acetamide and 5 mM (JSM-6360 LV instrument).

2.6. Fourier Transfer Infrared Spectroscopy (FTIR).

Thermo Fisher Nicolet IS10 was used to take the FTIR spectroscopy measurements, which were used to confirm and approve the chemical composition of the acetamide substance (KBr). A data table created from FTIR spectra that were published in the literature was integrated with the FTIR data. The mild steel coupons that had spent six hours submerged in 100 mL of $1 \times 10^{-3}\ M\ urea + 5\ mM\ KI$ inhibitors were removed and dried. Using a sharp blade, the thin layer formed on the metal surfaces was carefully scraped and then extensively mixed with KBr to make it consistent throughout. By scanning the sample throughout a 400–4000 cm^{-1} wave number range, the inhibitors' thin film produced leftovers as well as their powder forms, were analyzed.

2.7. Density Functional Theory Studies.

Recently, conceptual calculations to simulate experimental results have been conducted. Investigating the chemical reactivity of the acetamide molecule involves applying the traditional theory of Becke's three-parameter hybrid functional (B3LYP) level using a Gaussian 09W version with 6-311G+(d,p) as the reference set [22]. Equations 4 to 8 below were used to calculate the quantum parameters of the investigated approach, including the energy of the highest occupied molecular (E_{HOMO}), energy of the lowest unoccupied molecular orbital (E_{LUMO}), energy gap (ΔE_{L-H}), dipole moment (μ), absolute hardness (η), electronegativity (χ), global softness (σ), and number of electrons transferred (ΔN).

$$\Delta E = E_{LUMO} - E_{HOMO} \quad (4)$$

$$\sigma = \frac{2}{\Delta E} \quad (5)$$

$$\eta = \frac{\Delta E}{2} \quad (6)$$

$$\chi = \frac{-(E_{HOMO} + E_{LUMO})}{2} \quad (7)$$

$$\Delta N = \frac{(\chi_{Fe} - \chi_{inh})}{2 \times (\eta_{Fe} - \eta_{inh})} \quad (8)$$

Where, $\eta_{Fe} = 0\ eV$ and $\chi_{Fe} = 7$ in the case of iron,

2.8. Monte Carlo Simulations.

With the help of the adsorption locator module in the Materials Studio software, the adsorption energy of the tested substance on Fe is inferred from the MC simulation. COMPASS force field was used to carry out the optimal structures for the interaction of acetamide and water with the Fe (110) surface [21].

3. Results and Discussion

3.1. Weight Loss Techniques.

Weight-loss measurements were used to examine the rates of corrosion and the inhibition efficacy of the tested corrosion inhibitor at various concentrations $2 \times 10^{-4} - 1 \times 10^{-3}\ M\ acetamide\ and\ 5\ mM\ KI$) and varied temperatures (298-328 K). The experimental results are shown in **Table 1**. Both acetamide and acetamide + KI demonstrate good mild-steel corrosion inhibition. **Figure 1** depicts how the concentration of the inhibitors affects the rate of corrosion and, consequently, the effectiveness of the inhibition. As the concentration of the inhibitors rose, the inhibition got better, and the corrosion rate dropped. This demonstrates that inhibitor molecules are more thoroughly adsorbed onto the metal substrate as the concentration increases, leading to a wider surface coverage [23, 24]. It follows that the inhibition's effectiveness was concentration-dependent. As a result, there was little metal interaction with the acid solution. At $1 \times 10^{-3}\ M$, acetamide + KI exhibited the highest level of inhibitory efficacy; the inhibition efficiency was 80.64 % as compared to acetamide alone (68.95 %).

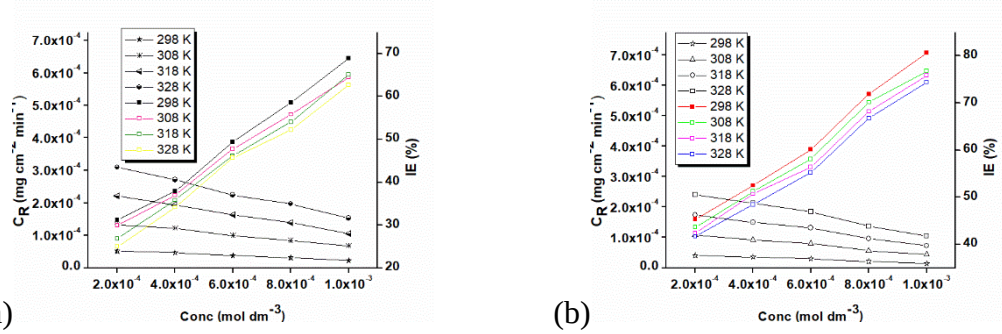

Figure 1 Effect of concentration and corrosion rate on the inhibition efficiency of **(a)** acetamide and **(b)** acetamide + KI on mild steel in 0.5 M H_2SO_4.

Table 1. Inhibition Efficiencies of mild steel corrosion using acetamide and acetamide + KI at different temperatures.

Percentage Inhibition Efficiency (%)

Conc	Acetamide				Acetamide + KI			
(M)	298 K	308 K	318 K	328 K	298 K	308 K	318 K	328 K
2×10^{-4}	31.24	29.92	26.86	24.93	45.28	43.61	42.36	41.65
4×10^{-4}	37.88	36.04	35.82	34.13	52.47	51.22	50.68	48.40
6×10^{-4}	49.40	47.76	46.18	45.65	60.13	58.10	56.38	55.25
8×10^{-4}	58.52	55.82	54.07	52.23	71.92	70.14	68.20	66.71
1×10^{-3}	68.95	64.44	65.14	62.67	80.64	76.71	75.87	74.39
$5.10^{-3}\ KI$	56.39	52.11	48.93	45.51	-	-	-	-

3.2. Effect of temperature.

Temperature significantly affects the corrosion rate and the inhibitors' effectiveness, especially in an acidic media. With higher temperatures, corrosion rates drastically rise [25-27]. To completely comprehend the studied inhibitor's protective performance, the inhibitor's corrosion rate and inhibitory effectiveness were assessed at various temperature ranges (298-328 K) (**Table 1**). The maximal inhibitory efficacy of the tested inhibitor was observed at 298 K, and when the temperature was elevated, this efficacy steadily reduced. The evaluated inhibitor did not perform well in terms of protection at the greatest temperature. These findings suggest that interactions were not made possible by the rise in temperature, which led to a decline in the effectiveness of the protective shield.

3.3. Kinetic and thermodynamics considerations.

The activation parameters of the corrosion process were determined using Arrhenius Equation (9) (**Figure 2**): The breakdown of mild steel requires time because inhibitory processes have a larger activation energy (Ea) than uncontrolled ones [28]. Additionally, the Ea rose along with the concentration of the inhibitor. This indicates that as the concentration increases, the inhibitor's physical barrier to the corrosion process strengthens [29,30]. As the temperature rises, less inhibitor molecules are able to bind to the metal surface, increasing the rate of corrosion. The values of the enthalpy of activation (ΔH_{ads}) and entropy of activation (ΔS_{ads}) can be determined using the transition state theory equation (Equation (10)):

$$lnC_R = lnA - \frac{Ea}{RT} \quad (9)$$

$$In\left(\frac{C_R}{T}\right) = \left(\frac{R}{Nh}\right) exp\left(\frac{\Delta S_{ads}}{R}\right) exp\left(\frac{-\Delta H_{ads}}{RT}\right) \quad (10)$$

where, C_R is the corrosion rate, A is Arrhenius constant or Pre-exponential factor, $R(8.314 J\ mol^{-1}K^{-1})$is the universal gas constant, T is absolute temperature, h is the plank's constant, and N is Avogadro's number.

Figure 3 depicts a plot of ln $\frac{C_R}{T}$ versus $\frac{1}{T}$. **Table 2** displays the values for activation-enthalpy (ΔH_{ads}) and activation-entropy (ΔS_{ads}). The positive ΔH_{ads} values [12] show the mild steel dissolving process to be endothermic. The rise in the ΔH_{ads} with increasing inhibitor concentration shows that the low rate of corrosion is mostly caused by the kinetic characteristics of activation. The values of the ΔH_{ads} range from 43.2 to 50.3 $kJ\ mol^{-1}$ with and without the addition of ($1 \times 10^{-3}\ M$) and/or 5 mM KI of acetamide (**Table 2**).

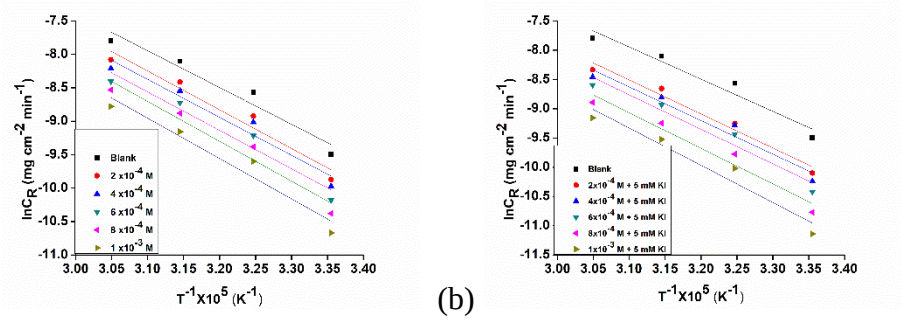

(a) (b)

Figure 2. Arrhenius plots of **(a)** acetamide alone and **(b)** acetamide + KI for mild steel in 0.5 M H_2SO_4 solution at various temperatures for 6 h.

The corrosion of mild steel controlled by the investigated inhibitors also demonstrated a number of water molecules on the mild steel surface being displaced by inhibitor molecules, according to the large negative values of ΔS_{ads} [31,32].

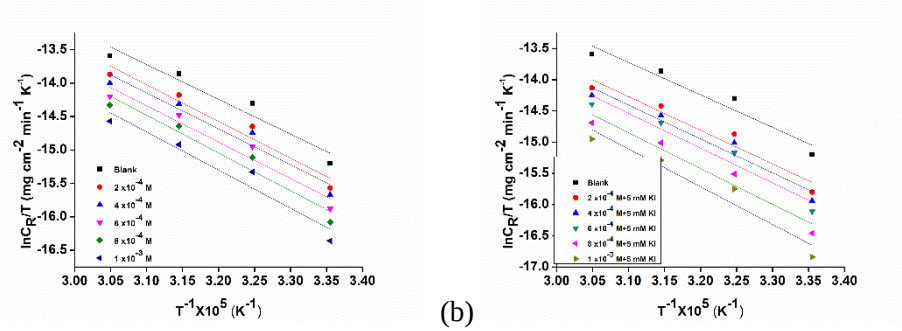

Figure 3. Transition state plots of **(a)** acetamide alone **(b)** acetamide + KI for mild steel in 0.5 M H_2SO_4 solution at various temperatures for 6 h.

Table 2. Values of kinetic and thermodynamic parameters of mild steel corrosion inhibition using acetamide and acetamide + KI.

Conc.	Acetamide			Acetamide + KI		
/(M)	Ea /(kJmol^{-1})	ΔH_{ads} /(kJ mol^{-1})	$-\Delta S_{ads}$ /(J mol^{-1})	Ea /(kJmol^{-1})	ΔH_{ads} /(kJ mol^{-1})	$-\Delta S_{ads}$ /(J mol^{-1})
Blank	45.7	43.2	177.6	45.7	43.2	177.6
0.0002	48.2	45.7	172.6	48.3	44.8	177.4
0.0004	47.2	44.6	176.9	47.8	45.2	177.3
0.0006	47.8	45.2	176.7	49.0	46.2	175.1
0.0008	49.6	46.9	172.5	50.5	47.6	173.4
0.001	50.2	47.4	173,1	52.9	50.3	167.3

3.4. Adsorption isotherm.

The barrier-shielding layer that protects the electrode surface is connected to the adsorption process (S_c). Equation (11), which connects the inhibitor concentration (C) and surface coverage, was used to match the gravimetric values using El-Awady, Temkin, Freundlich, Flory-Huggins, and Langmuir adsorption isotherm models (S_c). According to [33], the Langmuir adsorption isotherm, which accurately portrays the inhibitor-adsorption mechanism, was designed as the most suitable adsorption model in light of the high correlation coefficient (R^2) (**Figure 4**): The Langmuir equation is written out as follows:

$$\frac{C}{S_c} = \frac{1}{K_{ads}} + C \qquad (11)$$

where C is the inhibitor concentration, S_c is the degree of surface coverage, K_{ads} is the adsorptive equilibrium constant

The free adsorption energy (ΔG_{ads}) was computed based on Equation (12):

$$\Delta G_{ads} = -RTln(55.5K) \qquad (12)$$

Where, T is the absolute temperature, R is the universal gas constant, and the number 55.5 indicates the molar concentration of water.

The adsorption strength of the inhibitor increases with increasing (more negative) K_{ads} value, but adsorption is more spontaneously induced with decreasing (positive) ΔG_{ads}, value. The studied inhibitor exhibits a physical adsorption activity, as shown by the decreased ΔG_{ads}, value, as reported in **Table 3** [34].

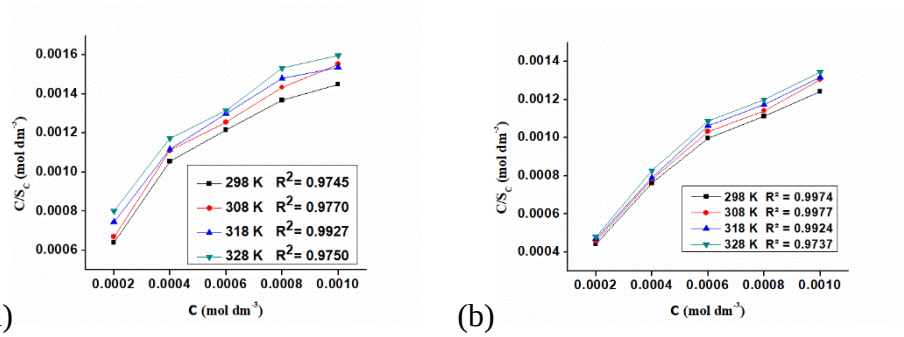

Figure 4. Langmuir plots for mild steel in 0.5 M H_2SO_4 solution of **(a)** acetamide alone **(b)** acetamide + KI at different temperatures.

Table 3. Parameters of Langmuir adsorption isotherm for acetamide and acetamide + KI as corrosion inhibitor of mild steel in 0.5 M H_2SO_4 at different temperatures.

Langmuir Isotherm	Temp.	R^2	Intercept	Slope	K_{ads}	ΔG_{ads}
Acetamide	298	0.9745	0.0002	1.3322	5.0000	-13.94
	308	0.9770	0.0004	1.2546	2.5000	-12.63
	318	0.9927	0.0006	1.2462	1.6667	-11.97
	328	0.9750	0.0008	1.0115	1.2500	-11.56
Acetamide + KI	298	0.9974	0.0001	1.4794	10.000	-15.66
	308	0.9977	0.0003	1.6982	3.3333	-13.37
	318	0.9924	0.0005	1.3649	2.0000	-12.45
	328	0.9737	0.0008	1.1650	1.2500	-11.56

3.5. Synergism effect parameters.

The following equation (13) was used to compute the synergism parameters based on the surface coverage values that were obtained.

$$\text{synergism parameters } (S_P) = \frac{1 - S_1 - S_2 + (S_1 \times S_2)}{1 - S_{1+2}} \quad (13)$$

Where, S_{1+2} is the degree of the surface coverage in their coexistence, S_1 and S_2 are the surface coverage in the individual presence of the organic and inorganic components, respectively.

The synergism parameters can be used to quantitatively express the synergistic inhibition effect between iodide ions and acetamide. **Table 4** shows that S_P values range from 0.55 to 0.79. This may be because nitrogen and oxygen atoms compete with the iodide ion for space on the metal surface, resulting in a lessened synergistic effect [35].

Table 4. Synergism parameter (S_P) for various concentrations of acetamide + KI as a mild steel corrosion inhibitor.

Acetamide (M)	KI (mM)	S_P			
		25°C	35°C	45°C	55°C
0.0002	5	0.55	0.60	0.65	0.70
0.0004	5	0.57	0.62	0.66	0.70
0.0006	5	0.55	0.60	0.63	0.66
0.0008	5	0.64	0.71	0.74	0.78
0.001	5	0.70	0.73	0.74	0.79

3.6. Electrochemical measurements.

The experimental results of the EIS studies of mild-steel corrosion at 298 K without, with, and with acetamide and acetamide + KI inhibitors are shown in **Table 5**. **Figure 5** illustrates how the presence of inhibitors in the 0.5 M H_2SO_4 environment significantly changed the mild steel's resistance responses. Increased substrate resistance, which was linked

to an increase in inhibitor concentration, was the cause of this variance. The Nyquist plots revealed a single loop in the impedance curves, showing that the charge transfer process and double-layer capacitance are primarily responsible for controlling the corrosion of mild steel in 0.5 M H_2SO_4 with and without protection. Additionally, these impedance spectra consistently shape across all concentrations studied, indicating that the corrosion mechanism is essentially unaltered [36]. With the addition of a single acetamide, the diameter of the semicircles marginally grows in comparison to the blank solution. However, when the two inhibitors are combined, the diameter of the curves increases significantly, demonstrating a stronger inhibitive ability with a synergistic impact. From the charge-transfer impedance, the double-layer capacitance and inhibitory efficiency (% IE) were calculated using equations (14) and (15) [37].

$$C_{dl} = \frac{1}{f_{max} \times 2\pi \times R_{ct}} \quad (14)$$

Where, f_{max} = the frequency value at which the imaginary component of the impedance is greatest

C_{dl} = double-layer capacitance,

$$\%\, I.E_{EIS} = \frac{[R]_{ct(inh)} - [R]_{ct(uninh)}}{[R]_{ct(inh)}} \times 100 \quad (15)$$

Where, $R_{ct(uninh)}$ (Ωcm^2) and $R_{ct(inh)}$ (Ωcm^2) = charge transfer resistances with and without inhibitor, respectively.

Table 5 shows that the charge-transfer resistance (R_{ct}) increased as the inhibitor concentration increased. Large charge transfer impedances are blamed for systems that corrode gradually [38]. The C_{dl} value was found to drop from133.4 (2×10^{-3} M) to 118.8 µF cm^2 (1×10^{-3} M) and 119.8 (2×10^{-3} M) to 100 µF cm^2 (1×10^{-3} M) in the presence of the tested inhibitors, indicating that the layer thickness at 1×10^{-3} M is larger than that at 2×10^{-3} M. The observed decrease in the C_{dl}, which was attributed to a reduction in the local dielectric constant and/or the thickness of the electrical double layer, shows that the inhibitors adsorbed onto the material's interface with the outside world. The observed decrease in the C_{dl} value in a corrosive solution in the presence of increasing concentrations may be due to inhibitor adsorption onto the most active adsorption sites [39].

The results also showed that the % IE rose along with the inhibitor concentration. It shows that a synergistic effect provides efficient defense against mild steel corrosion in a 0.5 M H_2SO_4 media. This result displays the same pattern as the % IE identified by the gravimetric measurements.

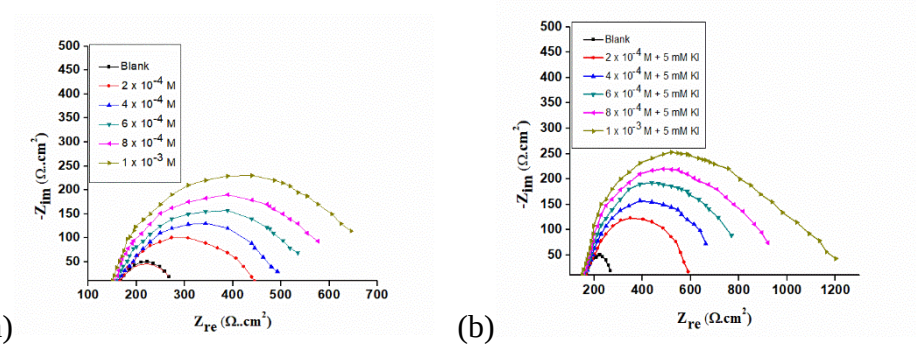

Figure 5. EIS Nyquist plots of the mild steel corrosion in 0.5 M H_2SO_4 and different concentrations of **(a)** acetamide alone **(b)** acetamide + KI at 298 K.

Table 5. EIS data for mild steel in 0.5 M H_2SO_4 containing various concentrations of acetamide and acetamide + KI at 25 ^{0}C.

Inhibitor	Conc (M)	R_s (Ω cm^2)	R_{ct} (Ω cm^2)	C_{dl} (μF cm^2)	% IE
Acetamide	0.5 M H_2SO_4	186.4	267.4	221.4	-
	2×10^{-4}	161.6	445.7	133.3	40.02
	4×10^{-4}	158.3	492.5	128.4	45.71
	6×10^{-4}	157.1	525.2	124.8	50.04
	8×10^{-4}	158.9	576.6	120.7	53.63
	1×10^{-3}	152.1	645.2	118.8	58.56
Acetamide + KI	2×10^{-4}	164.7	590.6	119.9	54.74
	4×10^{-4}	160.1	662.7	114.3	59.67
	6×10^{-4}	157.5	769.9	111.6	65.27
	8×10^{-4}	153.7	921.1	103.4	70.97
	1×10^{-3}	150.3	120.1	100.0	77.75

Figure 6a,b illustrates the comparable circuit schematic for fitting the actual EIS results for sulfuric acid with and without the inhibitor. The circuit elements for the data are the solution resistance (R_s), a constant phase element (C_{dl}), and the charge-transfer resistance (R_{ct}). The R_{ct} value indicated the efficiency of the electrons' motion over the contact. R_{inh} was used in conjunction with a C_{inh} as a model for the inhibitor adsorption, **Figure 6**b shows the environment impedance as R_s, the charge-transfer impedance as R_{ct}, the double-layer constant-phase element as C_{dl}, the adsorbed-layer impedance as R_{inh}, and the constant-phase element for the adsorbed layer as C_{inh}.. A complex nonlinear least squares simulation was employed, as previously reported [40], since an equivalent circuit is used to calculate the simulated values and for comparison with experimental data.

3.7. Scanning-electron-microscope (SEM)

Figure 7 shows SEM images of the mild-steel-coupon surface before (a), after (b), and after 6 hours at 298 K of immersion in 0.5 M H_2SO_4 solution and 1×10^{-3} M *acetamide* + 5 mM KI. While the coupon surface corroded severely in the corrosive solution and an abundance of corrosion porous products could be seen on the mild steel coupon surface in **Figure 7**b, the mild steel sample before immersion appeared smooth and showed some abrading scratches on the surface (**Figure 7**a). However, the mild-steel surface in the presence of the tested inhibitor had a smoother texture than the coupon subjected to the uninhibited acid solution, which suggests that the inhibitor was effective. The mild-steel surface in the presence of the tested inhibitor had a smoother texture than the coupon exposed to the uninhibited acid solution, suggesting that the inhibitor protected the coupon surface from the corrosive environment's attack. **Figure 7**c depicts the presence of an inhibitor. The findings of the other studies were supported by this discovery [41].

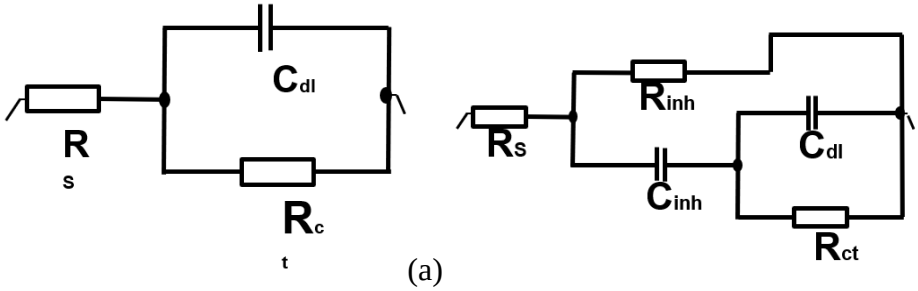

Figure 6. Equivalent circuit model for EIS measurements, **(a)** with acetamide and **(b)** without acetamide

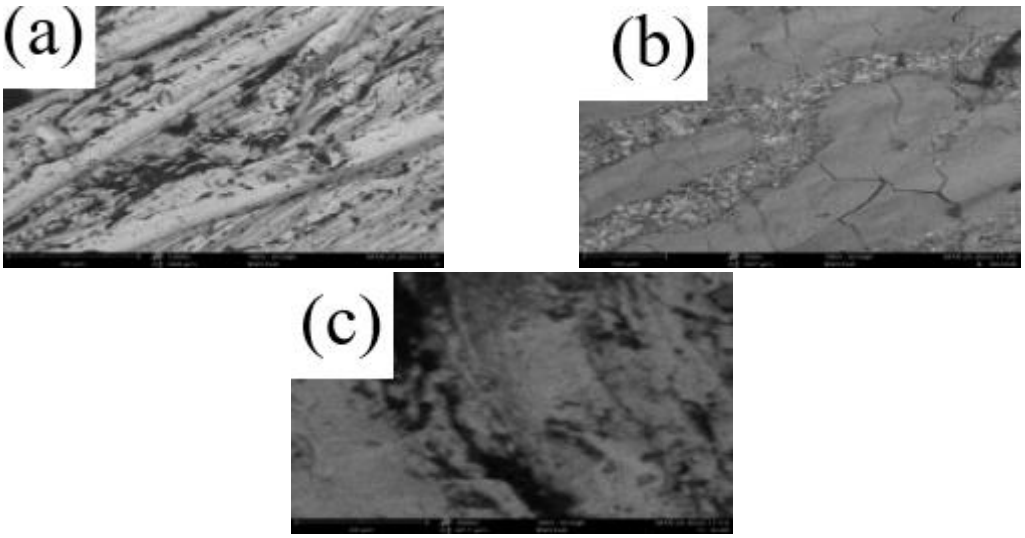

Figure 7. SEM images of mild steel **(a)** before immersion **(b)** after immersion in 0.5 M H_2SO_4, and **(c)** after immersion in 1×10^{-3} M acetamide + 5 mM KI immersion in solution for 6 h.

3.8. FTIR Study.

Figure 8 displays the FTIR spectrum of the film composed of acetamide $1 \times 10^{-3}\ M\ acetamide + 5\ mM$ KI that was generated on the surface of mild steel following immersion in 0.5 M H_2SO_4. From $1682.04\ and\ 1624.26$ to 1630.18 cm^{-1}, the C=O stretching frequency has changed to. From 3361.23 to 3385.65 cm^{-1}, the N-H stretching frequency has changed. From 582.79 to 460.86 cm^{-1}, the N-C=O deformation frequency has changed. This shows that the acetamide and Fe^{2+} on the surface of mild steel have coordinated through the oxygen atom of the C=O group and the nitrogen atom of the N-H group as well as N-C=O, resulting in the creation of the Fe^{2+} - acetamide complex. The peaks at 1087.17 and 1018.94 cm^{-1} are caused by K-I stretching. These findings suggest that there is KI produced on the metal surface. Hence, the FTIR study concludes that the protective film consists of KI and Fe^{2+} - acetamide complex produced on the metal surface [42].

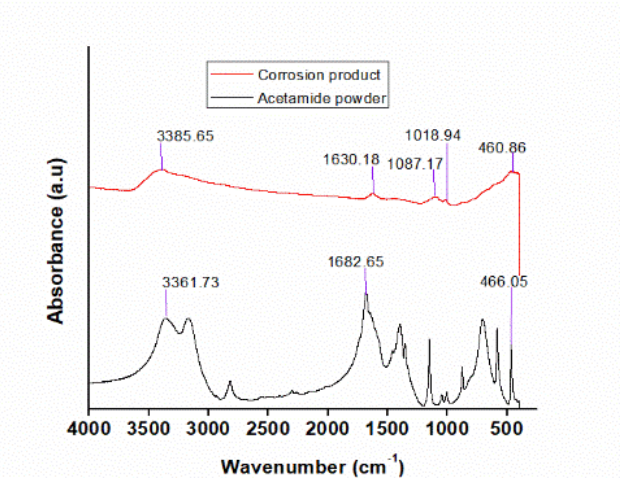

Figure 8. FTIR spectrum of acetamide powder and corrosion product.

3.9. Quantum chemical computations.

Frontier molecular orbital theory (FMOT) can be used to investigate the capacity of the synthesized inhibitor to adsorb on the mild-steel-coupon surface from the perspective of quantum-chemical computation [43]. The tested inhibitor's adsorption may be caused by donor-acceptor interactions. In this case, electrons are transferred from the organic compound's high-

electron-density centers (i.e., regions of highly electronic distributions) to the surface of mild steel's vacant 3d orbital (iron surface). **Table 6** shows and describes the quantum chemical parameters obtained from the tested inhibitor's gas and solvent phases optimization (**Figure 9**). E_{HOMO} demonstrates the tested inhibitor's capacity to donate electrons. A lower E_{LUMO} value indicates the molecules' capacity to take electrons from the iron's back donation and increase the binding energy between the metal and the inhibitor.

The tested inhibitor's ability to adhere to the metal surface is improved by higher E_{HOMO} and lower E_{LUMO} [44]. **Table 6** shows that when the number of inhibitor chemicals under investigation increases, the E_{HOMO} increases. This suggests that acetamide is a potent corrosion inhibitor and is in good agreement with the experimental data. The chemical response is determined by the energy gap (ΔE) values. In terms of reactivity, the molecule is more reactive toward the substrate surface, the higher its inhibitory efficiency, and the smaller the ΔE, the more stable it is. Acetamide, therefore, forms a stable compound with the Fe substrate. The dipole moment (μ) is brought on by the nonuniform surface charge distribution of the molecule's atoms. The inhibitor molecule is supported by the lowering magnitude of the dipole moment.

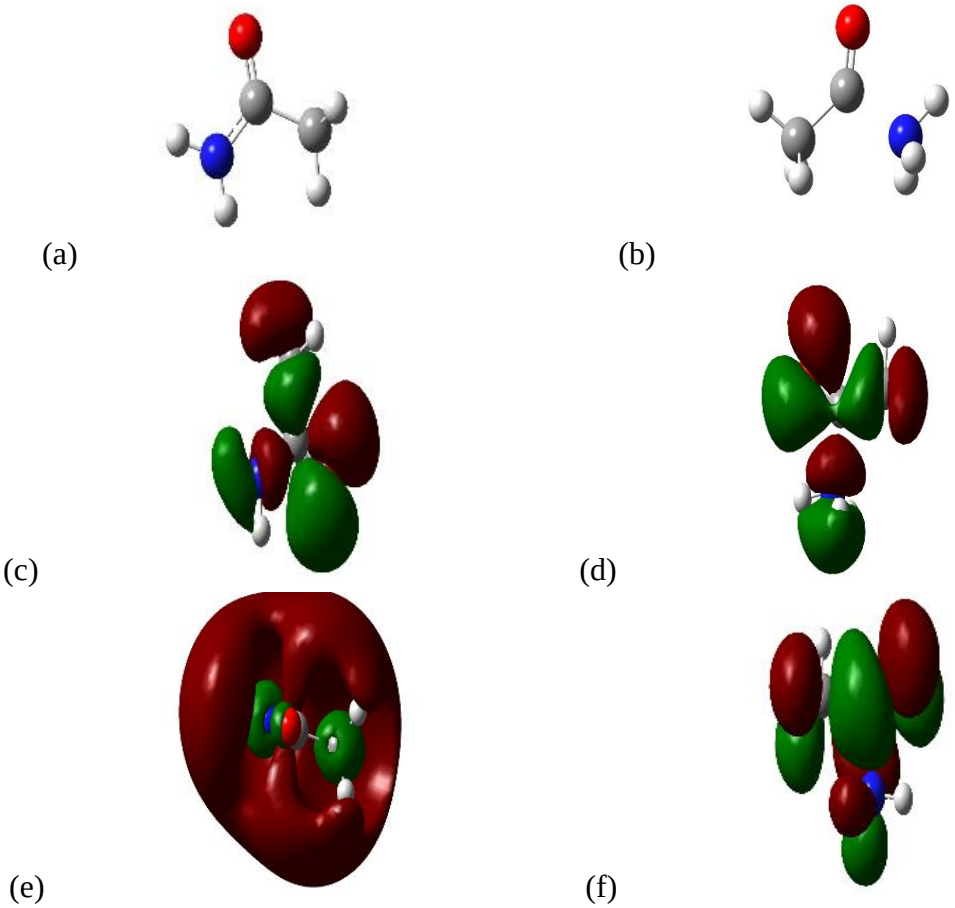

Figure 9. Optimized HOMO and LUMO structures of the acetamide **(a,c,e)** and protonated acetamide **(b,d,f)** respectively.

The soft molecule in the hard-soft acid-base concept has lower ΔE values and greater basicity, whereas the opposite is true when comparing the hard molecules. Due to its simpler electron transfer, the soft (σ) molecule has greater adsorption capacity and is a better corrosion inhibitor than the hard (η) molecule. According to Lukovit's research, the inhibition performance improves as a function of the electron transfer when the number of electrons (ΔN)

is less than 3.6. The fraction of electron transport (ΔN) increases with corrosion inhibitor strength. The highest adsorption ability of the tested inhibitor, as previously stated by the experimental results [45], is confirmed.

Table 6. Quantum chemical parameters of acetamide in the gas and solvent phases at B3LYP/6-311G+(d,p)

Phase	E_{HOMO}	E_{LUMO}	ΔE (eV)	σ (eV^{-1})	χ (eV)	η (eV)	ΔN (eV)	μ (Debye)
Gas	-0.264	-0.010	0.254	0.127	0.137	7.88	0.44	3.97
Solvent	-0.526	-0.252	0.274	0.137	0.389	7.31	0.45	5.45

3.10. Mulliken charges.

The tested inhibitor's adsorption centers were identified using Mulliken charges. The more negatively charged an atom is, the more readily it may transfer electrons [7]. N and O atoms are electron-donating sites in the investigated inhibitor molecule, as shown in **Table 7**. These atoms have the capacity to create coordination bonds with the metal surface.

Table 7. Fukui indices calculated B3LYP/6-311G+(d,p) of acetamide.

Inhibitor	Mulliken - Nucleophilic (F^+)		Mulliken- Electrophilic (F^-)	
	Atom	Charge	Atom	Charge
Acetamide	N1	-0.344	N1	-0.323
	C2	0.406	C2	0.440
	C3	-0.195	C3	-0.195
	O4	-0.603	O4	-0.531

3.11. Monte Carlo simulation.

The adsorption of inhibitor molecules on the metal surface can be studied using the MC simulation method. The optimal arrangements for urea and water adsorption on Fe (110) substrates are shown in **Figure 10**, and **Table 8** provides more specific data. Urea and $ureaH^+$ adsorb tightly and lie parallel to the Fe (110) surface, as can be seen from the photos in **Figure 10**. These are caused by coordinate bonds, which are created when inhibitor molecules give electrons to the iron's vacant d-orbital or accept them from iron by way of molecules' heteroatoms. The adsorption of inhibitors on the metal surface in a solution involves the quasi-substitution of inhibitor molecules to water molecules. The differential adsorption energy, or dE_{ad}/dN_i, represents the energy required to remove an adsorbate of a specific component. The water molecule can be gradually replaced by inhibitor molecules due to the low absolute value of dE_{ad}/dN_i for H_2O in **Table 8**. The most crucial adsorption parameter is adsorption energy, which consists of two components: the energy required to adsorb the sorbate onto the steel surface in its initial conformation (rigid adsorption energy) and a small deformation energy caused by the sorbate's relaxation on the surface of iron (Fe (110)). A strong adsorption behavior is reflected by adsorption energy with a high absolute value [46].

Additionally, since water's adsorption energy is lower than that of acetamide (−600.5 kJ mol^{-1}) (**Table 8**), water molecules on the metal surface are more quickly replaced by inhibitor molecules. As a result, the metal surface can be safeguarded. [47-49].

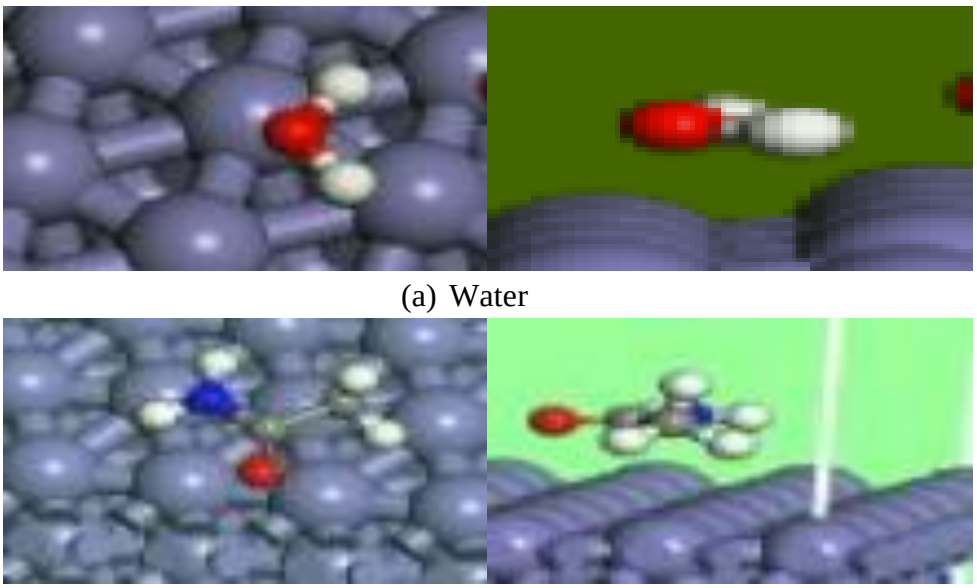

(a) Water

(b) Acetamide

Figure 10. Top and side view of the adsorption of the **(a)** water and **(b)** acetamide molecule on Fe (110) surface using the Monte Carlo simulation.

Table 8. Parameters calculated by the Monte Carlo simulation for adsorption of acetamide and water on Fe (110) (kJ mol^{-1}).

Compound	Energy				dE_{ad}/dN_i
	Total Energy	**Adsorption energy**	**Rigid Adsorption energy**	**Deformation energy**	
Acetamide	-1.573	-600.5	-541.6	-58.83	-15.83
Water	-174.9	-1.044	-176.7	-867.2	-103.9

4. Conclusions

Both the absence and presence of iodide ions were used to study the inhibitory effect of the acetamide compound on the corrosion of mild steel in 0.5 M H_2SO_4. With a synergism parameter range of 0.55 to 0.79, it has been discovered that iodide ions only slightly improve the inhibitive activity of acetamide, confirming their diminished impact. EIS graphs showed that as acetamide concentration is increased, R_{ct} values rise and C_{dl} values decrease. The ΔG_{ads} points to a physical type in the acetamide adsorption, which is in accordance with the Langmuir isotherm. Through the adsorption of acetamideH^+ molecules on the surface of mild steel, theoretical calculations demonstrate how acetamide prevents mild steel corrosion in the solvent phase.

Funding

This research received no external funding.

Acknowledgments

Declared none.

Conflicts of Interest

The authors declare no conflict of interest.

References

1. Umoren, S.A.; Solomon, M.M.; Obot, I.B.; Suleiman, R.K. Effect of intensifier additives on the performance of butanolic extract of date palm leaves against the corrosion of API 5L X60 carbon steel in 15 wt.% HCl solution. *Sustainability*, **2021**, *13*, 5569. https://doi.org/10.3390/su13105569.
2. Cao, S.; Liu, D.; Ding, H.; Wang, J.; Lu, H.; Gui, J. Task-specific ionic liquids as corrosion inhibitors on carbon steel in 0.5M HCl solution: An experimental and theoretical study. *Corros. Sci.*, **2019**, ***153***, 301–313. https://doi.org/10.1016/j.electacta.2008.10.025
3. Onyeachu, I.B.; Obot, I.B.; Sorour, A.A.; Abdul-Rashid, M.I. Green corrosion inhibitor for oilfield application I: Electrochemical assessment of 2-(2-pyridyl) benzimidazole for API X60 steel under sweet environment in NACE brine ID196. *Corros. Sci.*, **2019**, *150*, 183–193. https://doi.org/10.1016/j.corsci.2019.02.010.
4. Alhaffar, M.T.; Umoren, S.A.; Obot, I.B.; Ali, S.A.; Solomon, M.M. Studies of the anticorrosion property of a newly synthesized Green isoxazolidine for API 5L X60 steel in acid environment. *J. Mater. Res. Technol.*, **2019**, *8*, 4399–4416. https://doi.org/10.1016/j.jmrt.2019.07.051.
5. Zhang, Q.H.; Hou, B.S.; Li, Y.Y.; Zhu, G.Y.; Liu, H.F.; Zhang, G.A. Two novel chitosan derivatives as high efficient eco-friendly inhibitors for the corrosion of mild steel in acidic solution. *Corros. Sci.*, **2019**, ***164***, 108346. **01**, https://doi.org/10.1016/j.corsci.2019.108346.
6. Abdallah, M.; Fawzy, A.; Hawsawi, H.; Hameed, R.S.A.; Al-Juaid, S.S. Estimation of water-soluble polymeric materials (Poloxamer and Pectin) as corrosion inhibitors for carbon steel in acidic medium. *Int. J. Electrochem. Sci.*, **2020**, ***15***, 8129–8144, https://doi.org/10.20964/2020.08.73.
7. Mahdi, B. S.; Abbass, M. K. Mohsin, M. K.; Al-azzawi, W. K.; Hanoon, M. M.; Hliyil, M.; Al-kaabi, H.; Shaker, L. M.; Al-amiery, A. A.; Wan Isahak, W. R.; Kadhum, A. H.; Takriff. M. S. Corrosion inhibition of mild steel in hydrochloric acid environment using terephthaldehyde based on schiff base: gravimetric, thermodynamic, and computational studies. *Molecules* **2022**, *27*, 4857. https://doi.org/10.3390/molecules27154857.
8. Kadhim, A.; Al-Amiery, A.; Alazawi, R.; Al-Ghezi, M.; Abass, R. Corrosion inhibitors. A review. *Int. J. Corros. Scale Inhib*., **2021**, *10*, 54–67. http://dx.doi.org/10.17675/2305-6894-2021-10-1-3.
9. Hanoon, M.; Resen, A. M.; Al-Amiery, A. A.; Kadhum, A. A. H.; Takriff, M. S. Theoretical and experimental studies on the corrosion inhibition potentials of 2-((6-methyl-2-ketoquinolin-3-yl)methylene) hydrazinecarbothioamide for mild steel in 1 M HCl. *Prog. Color Colorants Coat*., **2022**, *15*, 21-33. https://doi.org/20.1001.1.20082134.2022.15.1.2.0.
10. Hashim, F.G.; Salman, T.A.; Al-Baghdadi, S.B.; Gaaz, T.; Al-Amiery, A.A. Inhibition effect of hydrazine-derived coumarin on a mild steel surface in hydrochloric acid. *Tribologia* **2020**, *37*, 45–53. https://doi.org/10.30678/fjt.95510.
11. Resen, A.M.; Hanoon, M.; Salim, R.D.; Al-Amiery, A.A. Shaker, L.M.; Kadhum, A.A.H. Gravimetrical, theoretical, and surface morphological investigations of corrosion inhibition effect of 4-(benzoimidazole-2-yl) pyridine on mild steel in hydrochloric acid. *Koroze. Ochr. Mater.* **2020**, *64*, 122-130. https://doi.org/10.2478/kom-2020-0018.
12. Sehmi, A.; Ouici, H.B.; Guendouzi, A.; Ferhat, M.; Benali, O.; Boudjellal, F. Corrosion inhibition of mild steel by newly synthesized pyrazole carboxamide derivatives and HCl acid medium: Experimental and theoretical studies. *J. Electrochem. Soc.*, **2020**, *15*, 155508. https://doi.org/10.1149/1945-7111/abab25.
13. Khalib, A. A.; Al-Hazam H. A.; Hassan, A. F. Inhibition of carbon steel corrosion by some new organic 2-hydroselenoacetamide derivatives in HCl medium. *Indones. J. Chem.*, **2022**, *5*, 1269 – 1281. https://doi.org/10.22146/ijc.72852.
14. Ade, S. B. Corrosion inhibition analysis of mild steel in various acid medium by amide (-$CONH_2$) group of organic compounds. *World. J. pharm. Res.*, **2022**, *11*, 1525-1535, https://www.researchgate.net/publication/358920129_CORROSION_INHIBITION_ANALYSIS_OF_MILD_STEEL_IN_VARIOUS_ACID_MEDIUM_BY_AMIDE_-CONH_2_GROUP_OF_ORGANIC_COMPOUNDS.
15. Umoren, S. A.; Solomon, M. M. Synergistic corrosion inhibition effect of metal cations and mixtures of organic compounds: A Review. *J. Environ. Chem. Eng.*, **2017**, *5*, 246-273. http://dx.doi.org/10.1016/j.jece.2016.12.001.

16. Feng, L.; Zhang, S;. Lu, Y.; Tan, B.; Chen, S.; Guo, L. Synergistic corrosion inhibition effect of thiazolyl-based ionic liquids between anions and cations for copper in HCl solution. *Appl. Surf. Sci.*, **2019**, *483*, 901–911. https://doi.org/10.1016/j.apsusc.2019.03.299.
17. Alamri, A. H. Experimental and theoretical insights into the synergistic effect of iodide ions and 1-acetyl-3-thiosemicarbazide on the corrosion protection of C1018 carbon steel in 1M HCl. *Materials*, **2020**, *13*, 5013. https://doi.org/10.3390%2Fma13215013.
18. Kangquan, V.; Ying, Z. Synergistic inhibition effect of diantipyrylmethane and potassium thiocyanate on mild steel corrosion in 1 M HCl solution. *Int. J. Electrochem. Sci.*, **2019**, *14*, 6999 – 7015. https://doi.org/10.20964/2019.08.57.
19. Alamiery, A.A.; Wan Isahak, W.N.R.; Takriff, M.S. Inhibition of mild steel corrosion by 4-benzyl-1-(4-oxo-4-phenylbutanoyl)thiosemicarbazide: gravimetrical, adsorption and theoretical studies. *Lubricants,* **2021**, *9*, 93. https://doi.org/10.3390/lubricants9090093.
20. ASTM G-31-72; Standard Recommended Practice for the Laboratory Immersion Corrosion Testing of Metals. *ASTM: Philaldelphia*, PA, USA, **1990**. *401*, https://www.slideshare.net/Wiltonifpe/astmg3172laboratoryimmersioncorrosiontestingofmetalscompresspdf.
21. Mashuga, M. E.; Olasunkanmi, L. O.; Ebenso, E. E. Experimental and theoretical investigation of the inhibitory effect of new pyridazine derivatives for the corrosion of mild steel in 1 M HCl. *J. Mol. Struct.* **2017**, *1136***,** 127−139. https://doi.org/10.1016/j.molstruc.2017.02.002.
22. Huong, D. Q.; Duong, T.; Nam, P. C. Effect of the structure and temperature on corrosion inhibition of thiourea derivatives in 1.0 M HCl solution. *ACS Omega*, **2019**, ***4***, 14478−14489. https://doi.org/10.1021/acsomega.9b01599.
23. Ouici, H. B.; Belkhouda, M.; Benali, O.; Salghi, R.; Bammou, L.; Zarrouk, A.; Hammouti, B. Adsorption and inhibition effect of 5-phenyl-1,2,4-triazole-3-thione on C38 steel corrosion in 1 M HCl. *Res. Chem. Intermed.*, **2015**, *41*, 4617. http://dx.doi.org/10.1007/s11164-012-0797-1.
24. Adejo, S.O.; Yiase, S.G.; Leke, L.; Onuche, M.; Atondo, M.V.; Uzah, T.T. Corrosion studies of mild steel in sulphuric acid medium by acidimetric method. *Int. J. Corros. Scale Inhib.*, **2019**, *8*, 50–61. http://dx.doi.org/10.17675/2305-6894-2019-8-1-5.
25. Fouda, A.; Tilp, A.; Al-Bonayan, A. Conocarpus Erectus Extract as an Eco-Friendly Corrosion Inhibitor for Aluminum in Hydrochloric Acid Solution. *Biointerface. Res Appl. Chem.*, **2021,** *11*, 10325 – 10340, https://doi.org/10.33263/BRIAC113.1032510340.
26. Hussein, R.; Abou-Krisha, M.; Yousef, T. Theoretical and Experimental Studies of Different Amine Compounds as Corrosion Inhibitors for Aluminum in Hydrochloric Acid. *Biointerface. Res Appl. Chem.*, **2021,** *11*, 9772 – 9785, https://doi.org/10.33263/BRIAC112.97729785.
27. Alamiery, A. A. Investigations on corrosion inhibitory effect of newly quinoline derivative on mild steel in HCl solution complemented with antibacterial studies. *Biointerface. Res Appl. Chem.*,**2022,** *12*, 1561 – 1568. https://doi.org/10.33263/BRIAC122.15611568.
28. Fouda,, A.S. ; Abdel Azeem, M.; Mohamed, S.A.; El-Hossiany, A.; El-Desouky. E. Corrosion Inhibition and Adsorption Behavior of Nerium Oleander Extract on Carbon Steel in Hydrochloric Acid Solution. *Int. J. Electrochem. Sci*. **2019,** *14*, 3932 – 3948, https://doi.org/10.20964/2019.04.44.
29. Tiwari, M.; Gupta, V. K.; Singh, R.A.; Ji, G.; Prakash, R. Donor−acceptor-type configured, dimethylamino-based organic push–pull chromophores for effective reduction of mild steel corrosion loss in 1 M HCl. *ACS Omega,* **2018**, *4*,4081–93. https://doi.org/10.1021/acsomega.8b00083.
30. Fouda, A. S.; El-Desoky, H. S.; Abdel-Galeil, M. A.; Mansour, D.; Niclosamide, D. Dichlorphenamide: new and effective corrosion inhibitors for carbon steel in 1M HCl solution. *SN Appl. Sci.*, **2021**, *3*, 287 | https://doi.org/10.1007/s42452-021-04155-w.
31. Shalabi, K.; Helmy, A.M.; El-Askalany, A.H.; Shahba, M.M. New pyridinium bromide mono-cationic surfactant as corrosion inhibitor for carbon steel during chemical cleaning: Experimental and theoretical studies. *J. Mol. Liq.* **2019**, *293*, https://doi.org/10.1016/j.molliq.2019.111480.
32. EL-Zekred, M. A.; Fouda, A. E. S.; Nofal, A. M.; Shalabi, K. Plantago Major Extract as an Environmentally Friendly Inhibitor for the Corrosion of L-80 Carbon Steel in 0.5 M H2SO4 Media. *Biointerface. Res Appl. Chem.*, **2021**, *11*, 12186 – 12201. https://doi.org/10.33263/BRIAC114.1218612201
33. Sliem, M.H.; El Basiony, N.M.; Zaki, E.G.; Sharaf, M.A.; Abdullah, A.M. Corrosion inhibition of mild steel in sulfuric acid by a newly synthesized schiff base: an electrochemical, DFT, and Monte Carlo simulation study. *Electroanalysis.* **2020**, *32*, 3145–3158. https://doi.org/10.1002/elan.202060461.

34. Aslam, J.; Aslam, R.; Lone, I.H.; Radwan, N.R.; Mobin, M.; Aslam, A.; Alzulaibani, A.A. Inhibitory effect of 2-Nitroacridone on corrosion of low carbon steel in 1 M HCl solution: An experimental and theoretical approach. *J. Mater. Res. Tech.* **2020,** *9*, 4061-4075, https://doi.org/10.1016/j.jmrt.2020.02.033.
35. Qiang, Y.; Qiang, Y.; Guo, L.; Zhang, S.; Li, W.; Yu, S.; Tan, J. Synergistic effect of tartaric acid with 2,6-diaminopyridine on the corrosion inhibition of mild steel in 0.5 M HCl. *Sci. Rep.* **2016**, *6*, 33305, https://www.nature.com/articles/srep33305.
36. Fouda, A.; El-Gharkawy, E.; Ramadan, H.; El-Hossiany, A. Corrosion Resistance of Mild Steel in Hydrochloric Acid Solutions by Clinopodium acinos as a Green Inhibitor. *Biointerface. Res Appl. Chem.,* **2021,** *11*, 9786 – 9803, https://doi.org/10.33263/BRIAC112.97869803.
37. Deyab, M. A. Electrochemical investigations on pitting corrosion inhibition of mild steel by provitamin B5 in circulating cooling water. *Electrochimica Acta* **2016**, *202*, 262–268. https://doi.org/10.1016/j.electacta.2015.11.075.
38. Wasim, M.; Shoaib, S.; Mubarak, N.M.; Inamuddin; Asiri, A.M. Factors influencing corrosion of metal pipes in soils. *Environ. Chem. Lett.* **2018**, *16*, 861-879, https://doi.org/10.1007/s10311-018-0731-x.
39. Appa Rao, B.V.; Narsihma Reddy, M. Formation, characterization and corrosion protection efficiency of self-assembled 1-octadecyl-1H-imidazole films on copper for corrosion protection. *Arab. J. Chem.* **2017**, *10*, S3270-S3283, https://doi.org/10.1016/j.arabjc.2013.12.026.
40. Meyer, Y.A.; Menezes, I.; Bonatti, R.S.; Bortolozo, A.D.; Osório, W.R. EIS investigation of the corrosion behavior of steel bars embedded into modified concretes with eggshell contents. *Metals* **2022**, *12*, 417. https://doi.org/10.3390/met12030417
41. Duarte, T.; Meyer, Y.A.; Osório, W.R. The holes of Zn Phosphate and hot dip galvanizing on electrochemical behaviors of multi-coatings on steel substrates. *Metals*, **2022**, *12*, 863. https://doi.org/10.3390/met12050863
42. Bedir, A. G. B.; Abd El-raouf, M.; Abdel-Mawgoud, S.; Negm, A. N.; El Basiony, N. M. Corrosion inhibition of carbon steel in hydrochloric acid solution using ethoxylated nonionic surfactants based on schiff base: electrochemical and computational investigations. *ACS Omega*, **2021**, *6*, 4300−4312. https://dx.doi.org/10.1021/acsomega.0c05476.
43. Yue, X.; Wei, Q.; Lu, Y.; Duan, M.; Wang, H.; Xie, J. The Synergistic Inhibition Effect between Imidazoline and 2-Mercaptoethanol on Carbon Steel Corrosion in CO2-saturated 3.5% NaCl solution. *Int. J. Electrochem. Sci.*, **2022,** *17* https://doi.org/10.20964/2022.05.55.
44. Fouda, A.S.; Ismail, M.A.; Temraz, A.M.; Abousalem, A.S. Comprehensive investigations on the action of cationic terthiophene and bithiophene as corrosion inhibitors: Experimental and theoretical studies, *New J. Chem.*, **2019**, *43*, 768–789. https://doi.org/10.1039/C8NJ04330B.
45. Saha, S.K.; Banerjee, P. Introduction of newly synthesized Schiff base molecules as efficient corrosion inhibitors for mild steel in 1 M HCl medium: An experimental, density functional theory and molecular dynamics simulation study, *Mater. Chem. Front.*, **2018**, *2*, 1674–1691. https://doi.org/10.1039/C8QM00162F.
46. Al-Sabagh, A.; El Basiony, N.; Sadeek, S.; Migahed, M. Scale and corrosion inhibition performance of the newly synthesized anionic surfactant in desalination plants: Experimental, and theoretical investigations, *Desalination*, **2018**, *437*, 45–58. http://dx.doi.org/10.1016/j.desal.2018.01.036.
47. Fouda, A. S.; Ismail, M. A.; Khaled, M. A.; El-Hossiany, A. A. Experimental and computational chemical studies on the corrosion inhibition of new pyrimidinone derivatives for copper in nitric acid, *Sci. Rep.*, **2022**, *12*,16089. https://doi.org/10.1038/s41598-022-20306-4.
48. Huong, D. Q.; Huong, N. T. L.; Nguyet, T. T. A.; Duong, T.; Tuan, D.; Thong, N. M.; Nam, P. C. Pivotal Role of heteroatoms in improving the corrosion inhibition ability of thiourea derivatives. *ACS Omega*, **2020**, *5*, 27655−27666. https://doi.org/10.1021/acsomega.0c04241.
49. Uzah,T. T.; Mbonu, J. I.; Gber, T. E.; Louis, H. Synergistic effect of KI and urea on the corrosion protection of mild steel in 0.5 M H_2SO_4: Experimental and computational insights. *Results in Chemistry*,**2023,** 5, 1-9. https://doi.org/10.1016/j.rechem.2023.100981